

Article

Deposition of Multicomponent AlTiCrMoN Protective Coatings for Metal Cutting Applications

Yin-Yu Chang ^{1,2,*} and Chih-Cheng Chuang ¹

¹ Department of Mechanical and Computer-Aided Engineering, National Formosa University, Yunlin 63201, Taiwan; 40271232@gm.nfu.edu.tw

² High Entropy Materials Center, National Tsing Hua University, Hsinchu 30013, Taiwan

* Correspondence: yinyu@nfu.edu.tw; Tel.: +1-886-5-6315332

Received: 6 June 2020; Accepted: 22 June 2020; Published: 28 June 2020



Abstract: The high potential of the protective coatings for metal machining applications using the physical vapor deposition (PVD) processes is one to be valued, and will accelerate development of the multicomponent coating design and increase the cutting efficiency. In this study, nanostructured AlTiCrMoN coatings in a multilayered structure were fabricated using cathodic-arc deposition (CAD). Controlling the cathode current of both CrMo and AlTi alloy targets in a nitrogen environment, multilayered AlTiN/CrMoN coatings were deposited. The AlTiN and AlTiN/CrMoN multilayered coatings exhibit a face-centered cubic (fcc) structure with columnar morphologies. The highest hardness of 35.6 ± 1.5 GPa was obtained for the AlTiN coating; however, the H^3/E^{*2} and H/E^* values were the lowest (0.124 and 0.059, respectively). The multilayered AlTiN/CrMoN coatings possessed higher H^3/E^{*2} and H/E^* values of up to 0.157 and 0.071, respectively. The present study investigated the cutting performance of end mills in the milling of SUS316L stainless steel. The cutting performance was evaluated in terms of cutting length and tool wear. Because of high resistance to adhesive and abrasive wear, the end mills coated with multilayered AlTiN/CrMoN showed less flank wear than monolithic AlTiN. The introduction of CrMoN sublayers improved the cutting tool life of AlTiN.

Keywords: AlTiN; CrMoN; hard coating; multilayer; wear; cutting

1. Introduction

In order to improve the tribological and mechanical performance, many tool materials are deposited with hard coatings on the basis of nitrides. Hard coatings, such as TiN, AlTiN and CrN, have been used extensively as protective coatings, which can improve the surface properties of the mechanical tools and prolong the service life [1–4]. These coatings enhance the resistance to wear and therefore increase the tool lifetime. Especially in the case of metal cutting, using advanced hard coatings has been a regular technique to meet the wide range of machining materials, especially for difficult-to-cut mold steel, stainless steel as well as composite materials [5]. In previous studies, AlTiN and AlCrN have been widely used as substitutes for TiN and CrN coatings for industrial applications. However, the high friction coefficient and poor resistance to brittle fracture of AlTiN coating is still a challenge for modern manufacturing. Compared to AlTiN coatings, AlCrN coatings exhibit excellent thermal stability and have a potential to improve oxidation resistance [6,7]. Therefore, many studies have focused on AlCrN coatings, which are a promising candidate for protective coating applications [8–12]. The introduction of Al atoms into the CrN phase showed a single-phase face-centered cubic (fcc) structure when the Al content was less than ~65 at.%; at higher Al contents, phase transformation from the fcc structure to the hexagonal closed packed (hcp) structure could be observed. Hence, adopting another transition element is an important technique to enhance mechanical properties and wear behavior of CrN and AlTiN. Because of the lower hardness of CrN coating (13~20 GPa), it limits its

applications in industry [13,14]. At present, multicomponent and multilayer design are important ways to increase the hardness of such nitride coatings. Recently, elements that are appropriate for anti-wear have raised great attention. Combined with TiN and CrN, it showed that the addition of molybdenum nitride (MoN) showed the successful improvement of mechanical properties and exhibited low friction force and improved wear resistance [15–20]. In addition, F.F. Klimashin et al. [21] showed that the single-phase CrMoN coatings possessed high hardness of 28–34 GPa, and the highest resistance against plastic deformation with $H^3/E^2 \approx 0.2$ GPa could be obtained. E.Y. Choi et al. [22] revealed that the hardness value 34 GPa of CrMoN coatings largely increased compared to 18 GPa of CrN coatings. The enhanced hardness values of CrMoN coatings were derived from the solid solution hardening. The average friction coefficient of CrMoN coatings was ~ 0.4 , and the decreased friction coefficient was explained by the formation of molybdenum oxide layer known as self-lubricating materials.

During the metal cutting processes, through-thickness cracks and chipping occurring in the hard nitride coatings are the main conditions for failure of the coated tools, and oxygen penetrates easily from the tool surface into the substrate and facilitates severe failure. As for the failure mode of the coated tool, it was found that the wear failure of the coating occurred in the sliding zone on the rake and flank faces. This wear failure could be induced by the effects of the sliding friction, crack propagation, adhesive wear and fatigue impact on the coated tool [23]. In particular, delamination and the formation of cracks in the hard coatings are the main mechanisms influencing the tool life and the reliability of metal-cutting tools. A.A. Vereschaka et al. had discussed various mechanisms of the formation of longitudinal cracks and delaminations in hard coatings on rake and flank tool surfaces, which varied based on the composition and architecture of the coatings [24]. They found that a balanced combination of hardness and ductility acted as an important consideration of designing hard coatings. To meet the rigorous cutting quality and reduction of tool wear, single-layer coating materials, such as AlTiN and AlCrN, are generally implemented on the tool for protection. Recently, multilayered hard coatings with periodic thickness in a nanoscale range have been studied extensively, and this approach uses the replacement of monolayer coatings by a hybrid architecture of multilayered and compositionally graded structures to meet the above requirement. Multilayered architecture, particularly with the alternating layers of materials with different properties, e.g., ductile metals and hard ceramics, acts as a crack inhibitor and thereby improves the fracture resistance. It exhibits an improved mechanical property combining high hardness, fracture toughness and crack resistance. Such multilayered coating properties usually depend on the chemical content and microstructure of each layer, interfacial adhesion and thickness of each layer [25–27]. In addition, carbon was introduced to form nanocomposite coatings, such as TiSiCN, TiAlCN and TiAlCrCN, to reduce adhesive wear and improve the cutting performance [28,29]. The presence of a barrier function in coatings could prevent interdiffusion of elements between the tool material and the material being machined. Physical vapor deposition (PVD) based on evaporation, magnetron sputtering and cathodic arc ion plating technologies are usually developed to supply ions that can assist in the formation of hard coatings. The presence of ions offers improved control of the film-substrate interface and the microstructure of films. Compared to other methods of PVD coatings, the cathodic arc ion plating method possesses the advantage of high degree of ionization of the arc plasma, which provides better control of film structure, high adhesion, efficient reactive deposition of compounds and uniform deposition over a variety of tool shapes [30–32]. In this study, monolithic AlTiN and multilayered AlTiN/CrMoN coatings were deposited by cathodic vacuum arc technique. The aim of this work was to study the mechanical properties and cutting performance of AlTiN and multilayered AlTiN/CrMoN coatings for end milling SUS316L stainless steel.

2. Experimental Details

In this study, monolithic AlTiN and multilayered AlTiN/CrMoN thin films were deposited on the samples of polished tungsten carbide (WC–Co, 7 wt.% Co, CAS Number: 12070-12-1) and machined with end mills with eight flutes (diameter = 8 mm). The tungsten carbide substrates were prepared by grinding and polishing to obtain an average surface roughness (R_a) = 0.1 ± 0.03 μm . The surface

roughness of the polished tungsten carbide was measured using a laser scanning microscope (VK-X100, Keyence Co., Osaka, Japan). Deposition was conducted in an industrial cathodic arc physical vapor deposition equipment (Surfwell Tech. Co., Taichung, Taiwan). Before deposition, the samples were ultrasonically cleaned in alcohol for 40 min and air dried. Three cathodes were vertically installed on flanges 90° apart, and pure Ti (CAS Number: 7440-32-6), AlTi (67 at.% of Al (CAS Number: 7429-90-5) and 33 at.% of Ti) and CrMo (90 at.% of Cr (CAS Number: 7440-47-3) and 10 at.% of Mo (CAS Number: 7439-98-7)) alloy targets were used for deposition of coatings. The samples were held by proper fixtures in the center of the coating machine and then placed on a single-axial rotation carousel. A rotation speed of 2 rpm was used to deposit the AlTiN and AlTiN/CrMoN. Before coating deposition, the substrates were ion cleaned by Ar (CAS Number: 7440-37-1) ion bombardment and further cleaned with Ti targets (metal ion cleaning) in Ar atmosphere to remove surface contamination.

The aforementioned ion cleaning and the following deposition processes were all conducted under continuous rotation of substrate holder to obtain uniform coatings. In order to obtain stoichiometric nitride coatings, the ratio of N/(Al + Ti + Cr + Mo) was controlled to be ~1. During the coating stage of nitrides, the samples were deposited in pure N₂ (supplied by nitrogen with a purity of 99.999 vol %, CAS Number: 7727-37-9) with the chamber pressure of 3.2 Pa, and a bias voltage of -120 V was applied. Radiant heaters were used to keep the substrate temperature at 280–320 °C. For the AlTiN coatings, TiN with thicknesses of ~0.3 μm was deposited as a bond coat. After the deposition of TiN, AlTiN/TiN multilayers (~0.2 μm) were deposited as transition layers, and then monolithic AlTiN was deposited as the top layer. For the deposition of multilayered AlTiN/CrMoN coatings, TiN and AlTiN/TiN were also designed as interlayers, and then AlTiN/CrMoN multilayers were deposited as the top layer. The cathode current of the targets was 70~140 A to control the composition of the coatings. The ratios of the AlTi/CrMo cathode current ($I_{[AlTi]}/I_{[CrMo]}$) were 1:1 and 2:1 to control the composition of AlTiN/CrMoN. The AlTiCrMoN-1 and AlTiCrMoN-2 were denoted for the AlTiN/CrMoN multilayered coatings with AlTi/CrMo cathode current ratios of 1:1 and 2:1, respectively.

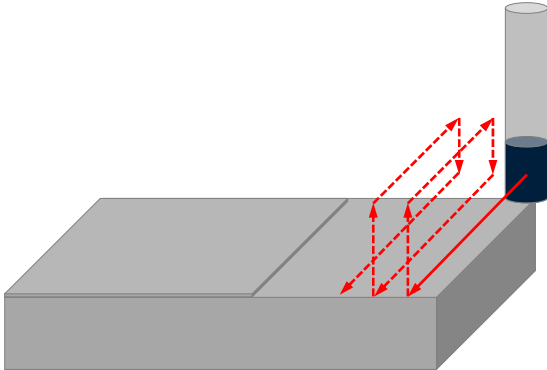
The phase structure of the coatings was investigated by X-ray diffraction (XRD; D8 Discover, Bruker Inc., Kanagawa, Japan) using Cu K α radiation as an X-ray source in parallel beam geometry. A low glancing incidence angle of 2° was selected. A JSM-7800F (JEOL Ltd., Tokyo, Japan) field emission scanning electron microscope (FESEM) with secondary electron image (SEI) was employed to reveal coating morphology and back scattering electron image (BEI) was used for the compositional contrast of the coating. The chemical composition of the coatings was also obtained by energy-dispersive X-ray spectroscopy (EDS). The nanostructure of the coating was observed by a high-resolution transmission electron microscope (HRTEM) equipped with an EDS system (JEOL JEM-2100F, Tokyo, Japan). The preparation of the transmission electron microscope (TEM) sample was conducted in a focused ion beam (FIB) cutting system and followed by a lift-out procedure.

The adhesion strengths between the WC-Co substrate and the coating were assessed by Rockwell C indentation tests with a load of 1470 N (150 kgf) according to the ISO 26443 standard. The nanoindentation tests were carried out on a nanoindenter (Nano Indenter G200, KLA Co., Milpitas, CA, USA) using diamond Berkovich indenters to measure the hardness (H) and Young's modulus (E) of the deposited coatings. The indenter loads increased at constant displacement rate of 10 nm/sec, until a maximum depth of 200 nm was achieved. The Poisson's ratio (ν) of the deposited coatings was assumed to be 0.25. The hardness and Young's modulus were obtained on a matrix of 2 × 3 indents by individual load-depth curves of up to six tests.

The machining tests were conducted on a machining center operated by a computer numerical control (CNC) milling machine (DMU 60T DECKEL MAHO, DMG MORI. Co., Ltd., Tokyo, Japan). The workpiece material SUS316L austenitic stainless steel (tensile strength = 570 MPa) was machined by end mills with different coatings (eight flutes, Ø8 mm). The hardness of the end mills was ~HRA 91. The cutting conditions are shown in Table 1. Cutting fluid of base oil was supplied. Tool specimens were inspected by a large depth-of-field optical microscope (VK-X100, Keyence Inc., Osaka, Japan) and scanning electron microscope (SEM, Phenom-World Pro-X, Thermo Fisher Scientific Inc., Waltham,

MA, USA) equipped with an EDS system. The milling process was interrupted for each experiment after completion and then value of the flank wear was measured.

Table 1. The cutting parameters of the coated end mills for machining SUS316L austenitic stainless steel.



Parameters	Value
Rotational speed, N (rpm)	9000
Cutting speed, V (m/min)	226.19
Feed rate, fz (mm/tooth)	0.0138
Axial depth of cut, ap (mm)	0.17
Radial depth of cut, ae (mm)	3

3. Results and Discussion

3.1. Microstructure Characterization of the Deposited Coatings

The XRD patterns obtained for the as-deposited AlTiN, AlTiCrMoN-1 and AlTiCrMoN-2 coatings are shown in Figure 1. All AlTiN, AlTiCrMoN-1 and AlTiCrMoN-2 coatings consist of cubic B1-NaCl structure and orientations of (111) (200), (220) and (311) planes were observed. For the AlTiN coating, the diffraction peak corresponding to the (111) reflection ($2\theta = 37.1^\circ$) indicated the existence of an fcc AlTiN solid solution [33–35]. The lattice parameter of the AlTiN was 0.419 nm, which was between the values of cubic TiN (0.424 nm, JCPDF file No.: #650565) and cubic AlN (0.405 nm, JCPDF file No.: #461200). The incorporation of Al to form fcc AlTiN solid solution was caused by the substitution of Ti atoms by smaller Al atoms.

The AlTiCrMoN-1 and AlTiCrMoN-2 coatings deposited at different cathode current ratios of AlTi/CrMo ($I_{[AlTi]}/I_{[CrMo]}$) also exhibited fcc crystal structure. The diffraction peaks of AlTiCrMoN-1 and AlTiCrMoN-2 coatings are also located between those of monolithic AlN and TiN. The diffraction peaks were similar to monolithic AlTiN except that the diffraction peak were shifted to higher angles, and a smaller lattice parameter of 0.418 nm was found. Similar results were also found in previous studies [36–38]. The peak shift was generally attributed to the lattice distortion due to the different atomic radius between Al, Ti Cr and Mo. Besides, no diffraction peaks of hexagonal AlN phase could be identified from the XRD patterns. AlN under thermodynamic equilibrium conditions forms a Wurtzite-type structure (hexagonal), whereas TiN has an fcc structure. In the multicomponent AlTiCrMoN, different growth directions of nitride grains appeared, showing that the cubic structure was formed by continuous growth of AlTiN and CrMoN when AlTi and CrMo alloy targets were evaporated in nitrogen environment. Stabilization of the cubic phase was observed.

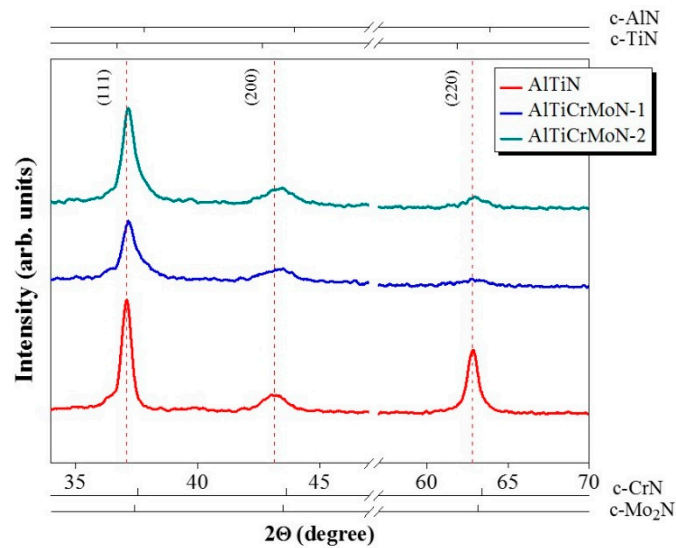


Figure 1. Glancing angle X-ray diffraction (XRD) pattern of the as-deposited AlTiN, AlTiCrMoN-1 and AlTiCrMoN-2 coatings.

The surfaces of all deposited coatings were similar in appearance to those investigated by using a laser scanning microscope, and all deposited coatings showed a higher R_a value of $0.25 \pm 0.1 \mu\text{m}$ than that of the polished substrates ($R_a = 0.1 \pm 0.03 \mu\text{m}$). The presence of micro-droplets was the main reason for the higher surface roughness observed on the cathodic arc evaporated coatings. Cross-sectional SEM micrographs, including SEI and BEI images, of the deposited AlTiN, AlTiCrMoN-1 and AlTiCrMoN-2 coatings are provided in Figure 2. As observed in the SEI images, the coatings exhibited columnar growth morphologies expanding from the initial growth on the substrate to the top layer of the whole coating. Especially for the AlTiN, the columns were slightly V-shaped with open column boundaries. Distinct columnar growth can be seen for conventional single-phase and cubic structured coatings, typical for the metallic and nitride thin films deposited at low temperature compared to melting point [39–43]. As shown in the SEI and BEI images of Figure 2, all deposited AlTiN, AlTiCrMoN-1 and AlTiCrMoN-2 coatings had TiN and TiN/AlTiN interlayers. The top layer of AlTiN/CrMoN and the interlayer of TiN/AlTiN exhibited multilayered structures. A multilayered structure could be formed by alternately depositing with different cathodic arc sources. The AlTiN/CrMoN top layer was deposited by alternate co-evaporation of CrMo and AlTi targets in a nitrogen environment. For all three coatings, the thicknesses of TiN and TiN/AlTiN interlayers were 0.28 and $0.23 \mu\text{m}$, respectively. The TiN/AlTiN interlayer, which was deposited by Ti and AlTi targets in nitrogen, was used as a transition layer from TiN to AlTiN and AlTiN/CrMoN top layers in order to obtain good adhesion strength. The total thicknesses of the AlTiN, AlTiCrMoN-1 and AlTiCrMoN-2 coatings were 1.43 , 1.48 , and $1.4 \mu\text{m}$, respectively.

Table 2 shows the EDS results, which revealed the chemical composition of the deposited AlTiN, AlTiCrMoN-1 and AlTiCrMoN-2 coatings. The ratio $N/(Al + Ti + Cr + Mo)$ was $0.97\sim 1.09$ to be stoichiometric. The highest $N/(Al + Ti)$ ratio was obtained for the AlTiN with atomic stoichiometry of $Al_{0.63}Ti_{0.37}N$. The $Al/(Ti + Al)$ atomic ratio in the $Al_{0.63}Ti_{0.37}N$ coating decreased to 0.63 compared with the $Al_{67}Ti_{33}$ cathode material, which was attributed to the different average ionization of Al and Ti and the lower atomic mass of Al that led to a lower Al density in the evaporated vapor [35,44]. For the AlTiCrMoN-1 and AlTiCrMoN-2 coatings, the results showed stoichiometric $Al_{0.29}Ti_{0.17}Cr_{0.46}Mo_{0.08}N$ and $Al_{0.38}Ti_{0.27}Cr_{0.30}Mo_{0.05}N$, respectively. At the AlTi/CrMo cathode current ($I_{[AlTi]}/I_{[CrMo]}$) of 1:1, which had the same AlTi and CrMo currents, the higher atomic ratio of Cr and Mo as compared to Al and Ti exhibited higher evaporation rate of the CrMo alloy target.

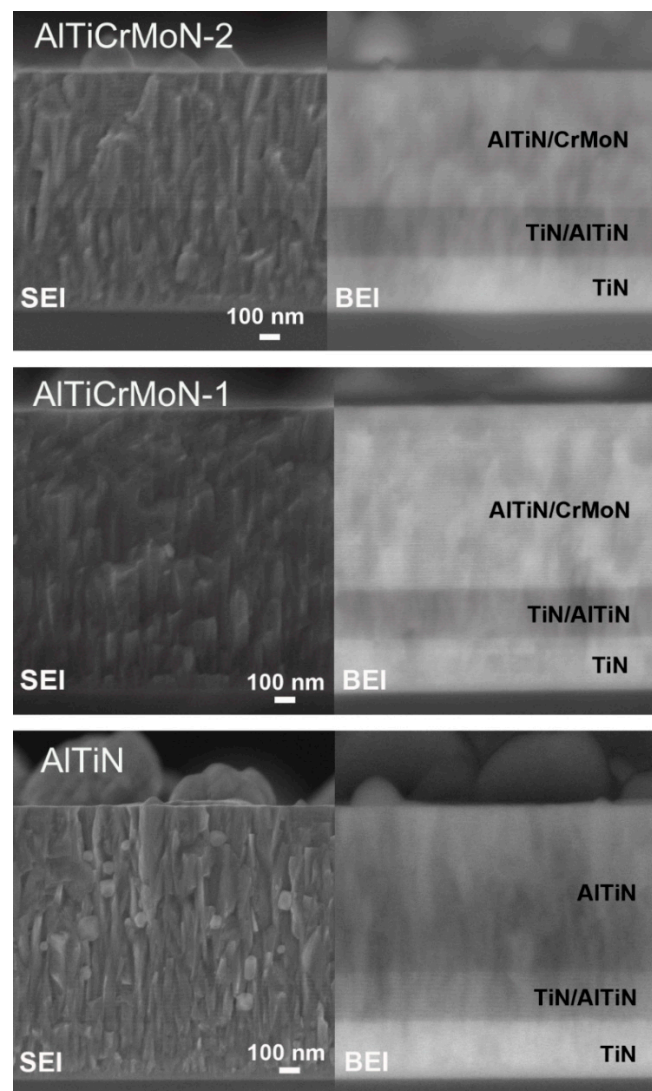


Figure 2. Cross-sectional scanning electron microscope (SEM) micrographs, including secondary electron image (SEI) and scattering electron image (BEI) images, of the deposited AlTiN, AlTiCrMoN-1 and AlTiCrMoN-2 coatings.

Table 2. Chemical composition of AlTiN, AlTiCrMoN-1 and AlTiCrMoN-2 coatings.

Coatings	Al(at %)	Ti(at %)	Cr(at %)	Mo(at %)	N(at %)
AlTiN	30.06	17.74	–	–	52.2
AlTiCrMoN-1	14.79	8.77	23.17	3.99	49.28
AlTiCrMoN-2	19.01	13.47	14.81	2.32	50.39

In order to describe the coating constitution, microstructure and compositional distribution, especially the TiN/AlTiN interlayer and the AlTiN/CrMoN top layer, the deposited AlTiCrMoN-2 coating was investigated by TEM. The cross-sectional TEM bright field image of the AlTiCrMoN-2 multilayered coating are presented in Figure 3. The selected-area electron diffraction (SAED) pattern is shown for the top AlTiN/CrMoN layer. It exhibits columnar structure without the presence of voids. The cross-sectional bright field TEM image showed well-adherent layers within the multilayered architecture and the interlayers of TiN/AlTiN and TiN. Previous studies [26,45,46] also indicated that the TiN interlayer and composition-gradient layers increased the adhesion strength and enhanced

the wear resistance of the AlTiN and multilayered TiAlSiN/TiN coatings. From the result of SAED pattern, the diffraction rings were identified as the reflections consistent with fcc NaCl type phases, and the pattern showed the characteristic diffraction rings of (111), (200) and (220). In agreement with the results obtained by XRD, the SAED patterns taken from the top multilayered AlTiN/CrMoN exhibited only fcc phases. The diffraction rings corresponding to AlTiN and CrMoN could not be easily separated owing to the small lattice misfit between the AlTiN and CrMoN sublayers [47,48].

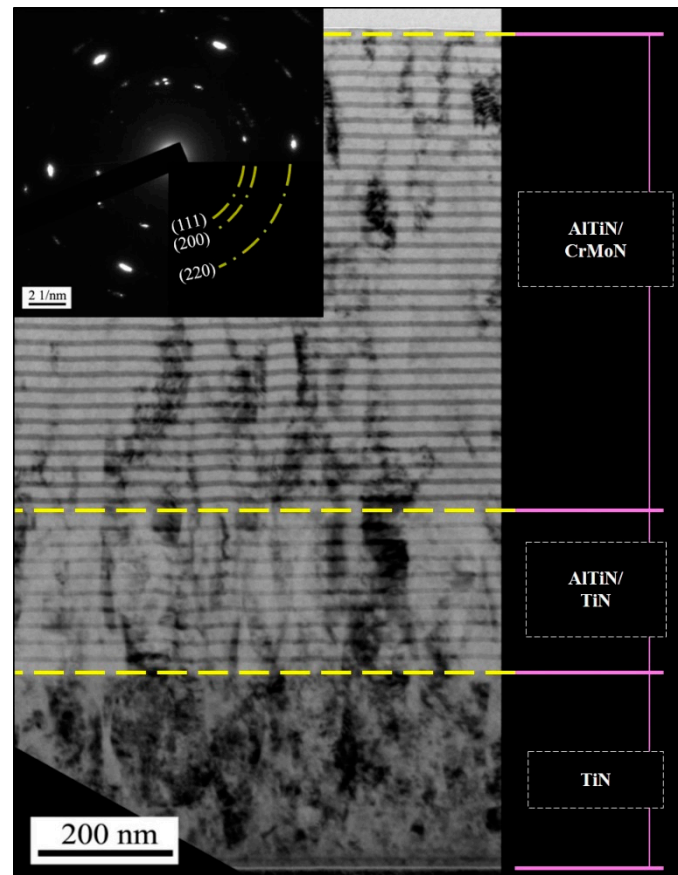


Figure 3. Cross-sectional transmission electron microscope (TEM) micrographs of the deposited AlTiCrMoN-2 coating and corresponding selected-area electron diffraction (SAED) pattern of the top multilayered AlTiN/CrMoN.

Figure 4 shows the cross-sectional HRTEM images of the top AlTiN/CrMoN multilayers of the AlTiCrMoN-2 coating with EDS line scan and fast Fourier transformation (FFT) of each AlTiN and CrMoN layer. The top layer of the AlTiCrMoN-2 coating showed pronounced layering structure with stacking of AlTiN and CrMoN layers. From the result of EDS line scan, the darker layers in the AlTiN/CrMoN nanolaminate coating could be marked as CrMoN and bright layers were AlTiN layers. The interfaces between AlTiN to CrMoN were coherent. B. Gao et al. [36] had shown that the ion energy would be influenced by the temperature during deposition, which affected the movement and diffusion of atoms in the multilayered films. In this study, we observed a distinct interface between the AlTiN and CrMoN when the deposition temperature was as low as 280–320 °C. According to the previous studies [49,50], the epitaxial growth of a multilayered film resulted from the lower interfacial energy during the deposition process. The stabilization of epitaxial growth occurs at small layer thicknesses in non-isostructural multilayers. The alternating AlTiN and CrMoN layers are perpendicular to the growth direction, shown as the bright and dark interval fringes with a bilayer thickness of 27.31 nm. The AlTiN/CrMoN multilayers of the AlTiCrMoN-2 coating was deposited by alternate evaporation of CrMo and AlTi targets in nitrogen atmosphere under AlTi/CrMo cathode current ratios of 2:1.

The higher the cathode current, the higher the evaporation rate of the target. Larger thickness of AlTiN was obtained, and the layer thickness ratio of AlTiN to CrMoN was 1.86. Assisted by the fast Fourier transformation (FFT) of square region in each AlTiN and CrMoN layer outlined in Figure 4, the d value measured from the selected AlTiN layer was 0.242 nm matches well with AlTiN (111), while the d value measured from the selected CrMoN was 0.238 nm for CrMoN (111).

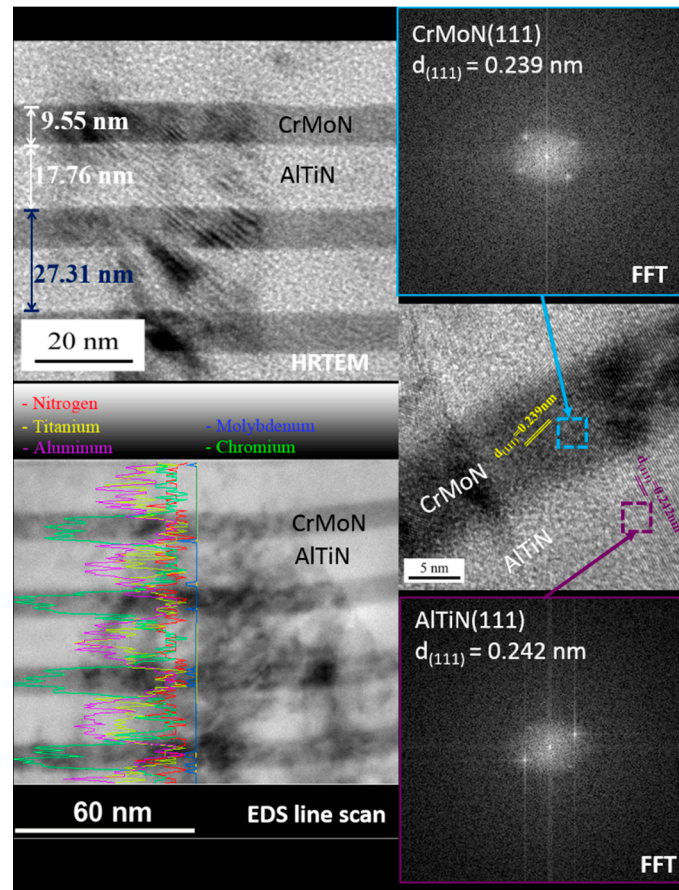


Figure 4. High-magnification cross-sectional high-resolution transmission electron microscope (HRTEM) images of the top AlTiN/CrMoN multilayers of the AlTiCrMoN-2 coating with energy-dispersive X-ray spectroscopy (EDS) line scan and fast Fourier transformation (FFT) of each AlTiN and CrMoN layer. Top left: HRTEM bright field image of the top AlTiN/CrMoN multilayers. Lower left: EDS line scan of the AlTiN/CrMoN multilayers. Top right: FFT image of the CrMoN layer. Lower right: FFT image of the AlTiN layer.

3.2. Mechanical Properties and Cutting Performances of the AlTiN, AlTiCrMoN-1 and AlTiCrMoN-2 Coatings

The adhesion strength between the hard-ceramic coating and the substrate material is one of the most important properties of PVD hard coatings as it influences the employment for mechanical applications such as metal cutting and forming, particularly for tribologically stressed cutting tools. The adhesion strength of all AlTiN, AlTiCrMoN-1 and AlTiCrMoN-2 coated samples were investigated using the Rockwell indentation test. The coating damage at the indentation imprint is assigned to four adhesion classes. Class 0 reveals acceptable adhesion. Class 1 shows no adhesive delamination; adhesion is acceptable. In the cases of class 2 and class 3, delaminations are present around the indentation imprint and adhesion is unacceptable. Figure 5 shows optical images to reveal the crack behavior of the AlTiN, AlTiCrMoN-1 and AlTiCrMoN-2 coated samples. Radial cracks, as indicated by the arrows in the figures, around the cone indentation were found on all coatings. No delaminations were present around the indentation imprint. The results showed strong adhesive strength (class 1). The radial cracks without chipping and delaminations exhibited good adhesion originating from

the proper TiN and TiN/AlTiN interlayer configurations. Our previous study [26] had shown that the improvement of adhesion strength and mechanical properties of multilayered AlTiCrN/TiSiN coatings were obtained by the interlayer design of CrN and composition-gradient transition layers. Y.W. Lin et. al. [51] had also shown that the TiZrN possessed improved adhesion strength and wear resistance by properly introducing a Ti interlayer. Compared to the single-layer coating, the design of adding composition-gradient interlayers and multilayers is proved to improve the mechanical properties and wear resistance.

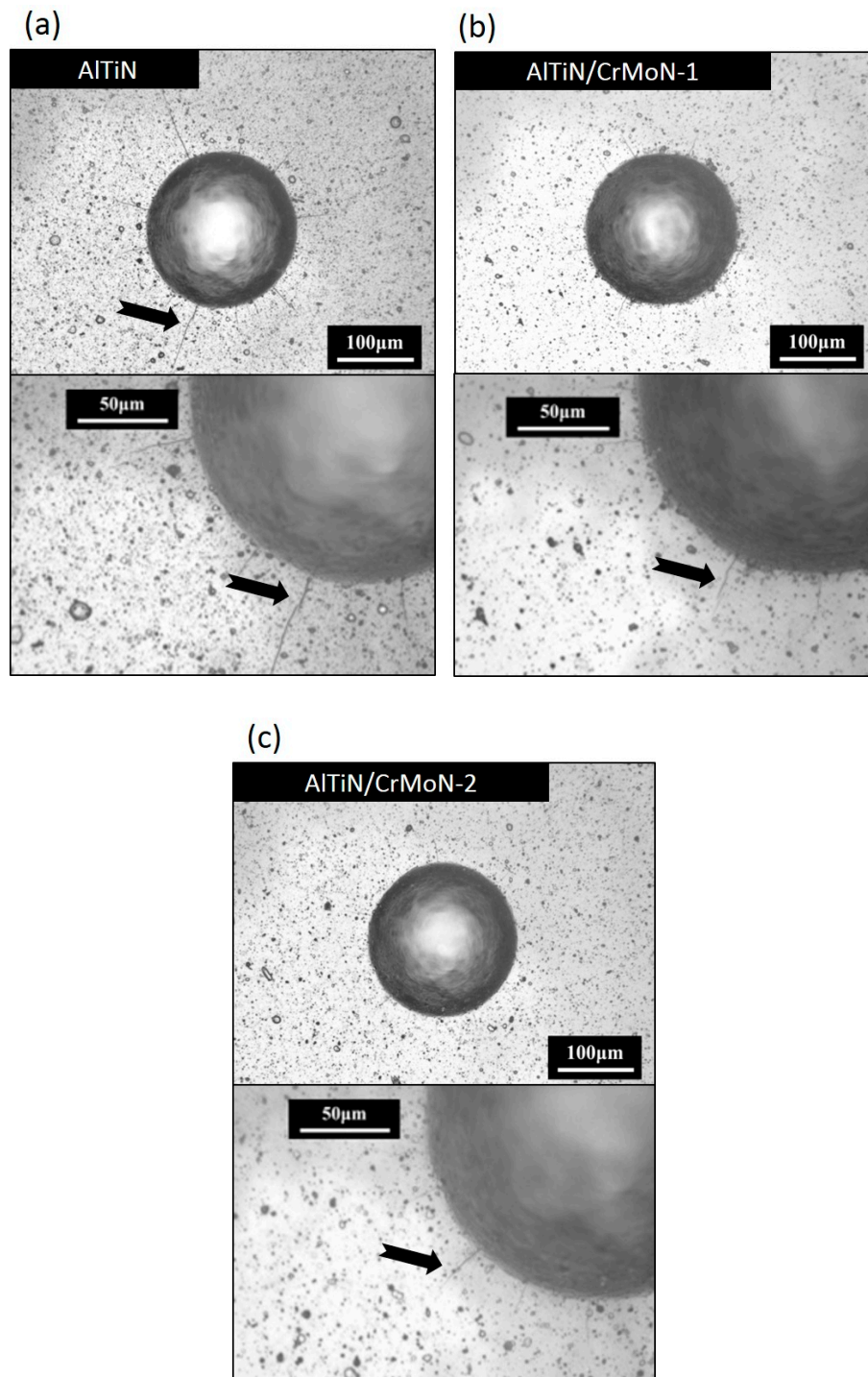


Figure 5. Optical images of the indentation crater of the (a) AlTiN, (b) AlTiCrMoN-1 and (c) AlTiCrMoN-2 coated samples after Rockwell indentation. Arrows indicate the radial cracks.

The hardness and Young's modulus of the deposited AlTiN, AlTiCrMoN-1 and AlTiCrMoN-2 coatings were measured using the nanoindentation test. Table 3 shows the measured hardness, Young's modulus, H/E^* and H^3/E^{*2} value of the coatings. The hardness of the AlTiN coating was 35.6 ± 1.5 GPa, which was higher than that of the AlTiN (32.47 GPa) coating synthesized by a filtered cathodic vacuum arc deposition method and the TiAlN (33.1 GPa) coating deposited by magnetron sputtering [3,5,52]. The AlTiCrMoN-1 and AlTiCrMoN-2 coatings displayed lower hardness of 29.4 ± 0.2 and 32.0 ± 1.5 , respectively. Higher values for both hardness and Young's modulus were found in the monolayer AlTiN coatings when compared with the multilayer AlTiCrMoN systems. Compared to the AlTiCrMoN-1 coating deposited under AlTi/CrMo cathode current ratios of 1:1, AlTiCrMoN-2 deposited under AlTi/CrMo cathode current ratios of 2:1 had higher hardness due to the higher Al and Ti contents in the film. The H/E^* and H^3/E^{*2} values of the deposited AlTiN were 0.059 and 0.124, respectively. Although the AlTiN possesses higher hardness than that of AlTiCrMoN-1 and AlTiCrMoN-2, higher values of H/E^* (0.068~0.071), which indicates a higher resistance to cracking [53–55], and H^3/E^{*2} (0.137~0.157), which indicates a higher resistance to plastic deformation, a major factor of coating's wear resistance property [54,56], were obtained for AlTiCrMoN-1 and AlTiCrMoN-2 coatings. E^* is expressed as $E/(1-\nu^2)$, where E and ν are the Young's modulus and the Poisson ratio, respectively. In this study, the AlTiCrMoN-2 coating with AlTiN/CrMoN multilayers had the highest H/E^* (0.071) and H^3/E^{*2} (0.157) among the deposited coatings. A recent study [57] also showed that the CrN/Si₃N₄ multilayered coatings with a high H/E^* and H^3/E^{*2} values exhibited high cracking resistance to improve friction and wear. The multilayer interfaces could reduce crack propagation and adhesion failure. Compared to the AlTiN coating, the AlTiCrMoN-1 and AlTiCrMoN-2 coatings with nanolayered structure of the AlTiN/CrMoN top layer had high H/E^* and H^3/E^{*2} that could be beneficial to enhance the tribological and cutting performances.

Table 3. Hardness, Young's modulus, H/E^* and H^3/E^{*2} value of the deposited AlTiN, AlTiCrMoN-1 and AlTiCrMoN-2 coatings.

Coatings	Hardness (GPa)	Young's Modulus (GPa)	H/E^*	H^3/E^{*2}
AlTiN	35.6 ± 1.5	565.0 ± 37.9	0.059 ± 0.007	0.124 ± 0.037
AlTiCrMoN-1	29.4 ± 0.2	404.8 ± 45.8	0.068 ± 0.009	0.137 ± 0.040
AlTiCrMoN-2	32.0 ± 1.5	428.6 ± 41.2	0.071 ± 0.011	0.157 ± 0.064

3.3. Comparison of the Cutting Performance of the End Mills Coated with the AlTiN, AlTiCrMoN-1 and AlTiCrMoN-2 Coatings

AlTiN, AlTiCrMoN-1 and AlTiCrMoN-2 coatings were deposited on the end mills for the cutting test. The experiments were conducted at a high cutting speed (V_c) of 226.19 m/min with a constant spindle speed of 9000 rpm on austenitic SUS316L stainless steel. The influence of AlTiN and multilayered AlTiCrMoN hard coatings on the wear behavior and cutting performance of end mills was investigated. When machining the difficult-to-cut austenitic stainless steel, in addition to abrasion wear, adhesion failure of the tungsten carbide tools was usually found. The challenge in cutting the austenitic stainless steel materials is the serious adhesion of the work piece material to the cutting edge, which causes early chipping of the end mills. Figure 6 presents the lifetime curves of average flank wear obtained with different tools at different cutting lengths. In this study, the flank wear of 60 μm was used as a criterion to evaluate the primary lifetime of the end mills. The results showed that the flank wear increased rapidly before the cutting length of 10 m. As shown in Figure 6, the cutting distance of the uncoated end mill is approximately 6 m due to severe wear, whereas the monolithic AlTiN coated end mill had longer lifetime, i.e., ~21.9 m. All AlTiN and multilayered AlTiCrMoN coated end mills had lower flank wear than the uncoated tools. By adding CrMoN to form a multilayered coating, the AlTiCrMoN-1 coated end mill outperformed the AlTiN. The AlTiCrMoN-2 with a multilayered AlTiN/CrMoN top layer possessed the longest tool life of 79.1 m. Table 4 shows a comparison of cutting performance of different coatings for machining austenitic stainless steels [58–62]. AlTiN, AlTiCrN and AlTiSiN

are usually used as the protective hard coatings for cutting stainless steels and resist thermal shock and severe abrasive wear at the tool-chip interface. Selective laser melting (SLM) and laser texturing before applying the PVD coatings were also used to improve the cutting performance. In this study, the multilayered AlTiCrMoN-2 coated tool outperformed the AlTiN by having a tool life 3.6 times longer than the AlTiN, and it possessed the best cutting performance.

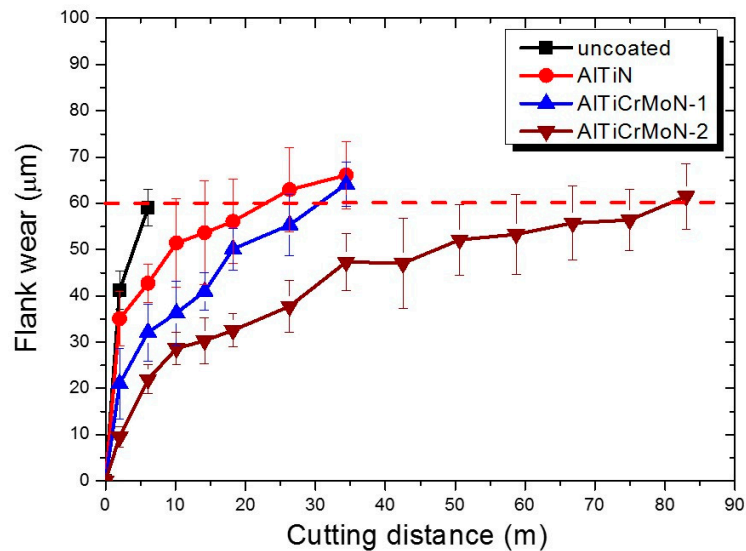


Figure 6. Average flank wear of the AlTiN, AlTiCrMoN-1 and AlTiCrMoN-2 coated end mills for machining SUS316L stainless steel with cutting distances to 82 m.

Table 4. Comparison of cutting performance of different coatings for machining austenitic stainless steels.

Coating	Deposition Method	Cutting Performance	Reference
TiAlN	Physical vapor deposition (PVD) with the selective laser melting (SLM) technique	Decrease of 10–20% in cutting forces, a decrease of 10–15% in cutting temperature and a high surface quality of the machined workpieces at the high cutting speed.	[54]
AlTiN	Cathodic arc vapor deposition technique	The nano-crystalline AlTiN coating outperformed the traditional AlTiN coating that almost doubled the tool life due to the reduction of the sticking of the stainless steel to the tool’s surface.	[55]
AlTiN AlTiCrN AlTiSiN	Cathodic arc vapor deposition technique	Effectively resists thermal shock and severe abrasive wear at the tool–chip interface due to the high H^3/E^2 ratio.	[56]
TiAlN	Cathodic arc vapor deposition with laser irradiation technique	The anti-adhesive wear properties of laser textured TiAlN coated tool were significantly improved over that of the conventional TiAlN.	[57]
TiN/MoN (Multilayer)	Magnetron sputtering	The numbers of drilling holes the coated drills were 4.2 times larger than that of uncoated high speed steel (HSS) drills. Adhesive friction and the formation of the build-up edge was avoided.	[58]
AlTiN/CrMoN (Multilayer)	Cathodic arc vapor deposition technique	The nanolayered AlTiCrMoN-2 coated tools outperformed the AlTiN that had a tool life 3.6 times longer than that of AlTiN. And it possessed the best cutting performance.	This study

Figure 7 shows the optical microscopic observations of worn faces of the uncoated and coated end mills after machining of SUS316L stainless steel tested during cutting lengths of 6 m, 34 m and 82 m.

Distinct abrasion was observed on the flank faces of the uncoated tools at the early cutting length of 6 m. The flank wear at the cutting edge resulted from the increasing cutting heat and friction wear during milling. The end mill blunted during the high-speed cutting process due to its poor heat resistance, which facilitated serious abrasion. After cutting a length of 34 m, the AlTiN and AlTiCrMoN-1 coated end mill had an average flank wear of $\sim 66 \mu\text{m}$ and $\sim 64 \mu\text{m}$, respectively, and showed obvious abrasion wear on the cutting edge, which caused the chipping and delamination of the coating, while smaller flank wear was obtained for the AlTiCrMoN-2 coated end mill. Previous studies [63,64] revealed that the failure mechanism of the AlTiN coated end mills included abrasion, chipping due to the thermal fatigue, adhesion of workpiece material with formation of build-up edge (BUE). After the protective coating had worn away, the tool substrate was exposed, leading to the adhesive BUE formation on the coated tools at high temperature. The AlTiCrMoN-2 with multilayered AlTiN/CrMoN top layer (layer thickness ratio of AlTiN to CrMoN = 1.86) had average flank wear of $\sim 61 \mu\text{m}$ after cutting length of 82 m, and possessed the lowest progression of tool flank wear. In addition, the AlTiCrMoN-2 coating possessed high H/E^* and H^3/E^{*2} values, which improved the wear resistance.

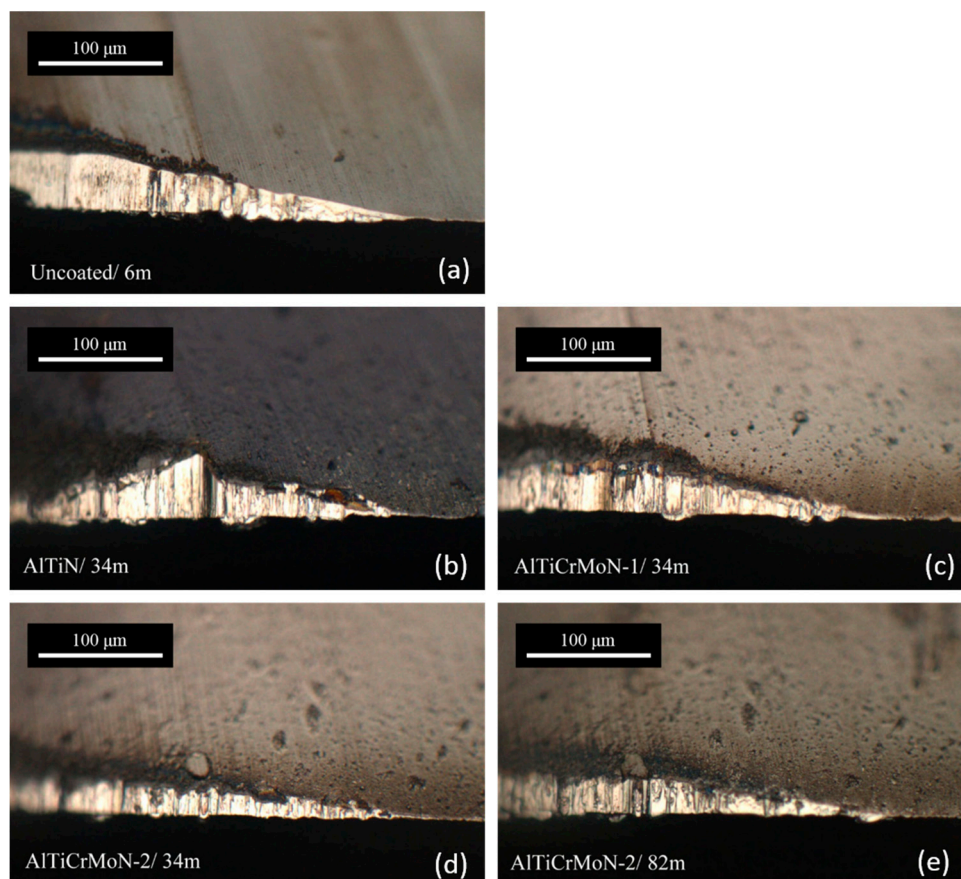


Figure 7. Tool wear images of the uncoated and AlTiN, AlTiCrMoN-1 and AlTiCrMoN-2 coated end mills after machining of SUS316L stainless steel after cutting lengths of 6 m, 34 m and 82 m. (a) Uncoated after cutting length of 6 m; (b) AlTiN after cutting length of 34 m; (c) AlTiCrMoN-1 after cutting length of 34 m; (d) AlTiCrMoN-2 after cutting length of 34 m; (e) AlTiCrMoN-2 after cutting length of 82 m.

Figure 8 shows the SEM image and EDS mapping results of the AlTiCrMoN-2 coated end mills after cutting length of 82 m when the flank wear exceeded $60 \mu\text{m}$. As displayed in the figure, the compositional EDS mapping images revealed the exposure of the tool substrate (W mapping) and the adhered material (Fe mapping). The machined material mainly adhered to coated end mills on the cutting edge of the flank wear zone. A small exposure area of the tool substrate (W mapping) was found at the cutting edge, indicating the excellent wear resistance of the AlTiCrMoN-2 with AlTiN/CrMoN multilayers

(bilayer thickness = 27.31 nm). Coating delamination and longitudinal cracking due to brittle failure are the major failure mechanisms of the cutting tool with hard coatings, especially in the case of AlTiN. The coating failure, wear and delamination on tool surfaces are based on the compositions and architectures of the coatings [24]. The coalesced top coating layer and gradient interlayers provided good adhesion strength of the hard coating to cutting tools and improved machining behavior [65,66]. In this study, the nanolayered AlTiCrMoN-2 coating had high H/E^* and H^3/E^{*2} values, which improved the resistance to plastic deformation and provided inhibition of crack formation and propagation, and outperformed monolithic AlTiN at high cutting speed. Therefore, the nanolayered AlTiCrMoN-2 coated tools possessed the best cutting performance among the investigated coatings and had the longest tool lifetime of the end mills.

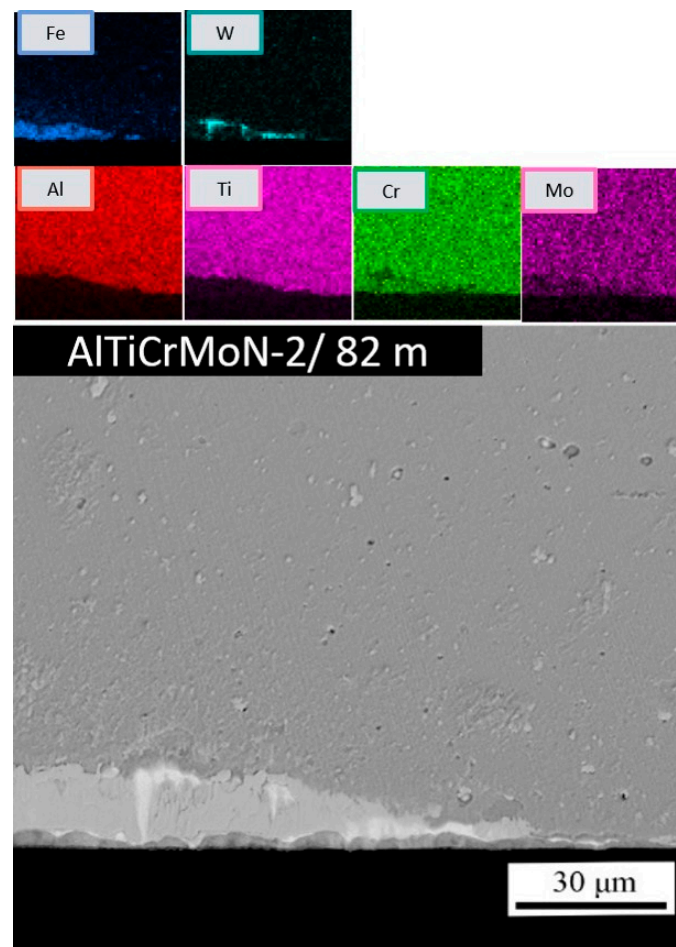


Figure 8. SEM image and EDS mapping results of the AlTiCrMoN-2 coated end mills after cutting length of 82 m.

4. Conclusion

In this study, $Al_{0.63}Ti_{0.37}N$, $Al_{0.29}Ti_{0.17}Cr_{0.46}Mo_{0.08}N$ and $Al_{0.38}Ti_{0.27}Cr_{0.30}Mo_{0.05}N$ coatings were synthesized by cathodic vacuum arc deposition using pure Ti, AlTi (67 at.% of Al and 33 at.% of Ti) and CrMo (90 at.% of Cr and 10 at.% of Mo) alloy targets. All deposited coatings possessed a B1–NaCl crystal structure, and all deposited coatings had TiN and TiN/AlTiN interlayers to obtain good adhesion strength. The $Al_{0.38}Ti_{0.27}Cr_{0.30}Mo_{0.05}N$ coating deposited using AlTi/CrMo cathode current ratio ($I_{[AlTi]}/I_{[CrMo]}$) of 2:1 possessed multilayered AlTiN/CrMoN structure with alternate growth of AlTiN and CrMoN. Larger thickness of AlTiN was obtained, and the layer thickness ratio of AlTiN to CrMoN was 1.86. The mechanical properties and cutting performance of the coated end mills in

milling of a SUS316L stainless steel was studied. Based on the results acquired, the main conclusions were drawn as follows:

The AlTiN coating possessed the highest hardness of 35.6 ± 1.5 GPa, however, their H/E^* and H^3/E^{*2} values were the lowest (0.059 and 0.124, respectively). The $Al_{0.38}Ti_{0.27}Cr_{0.30}Mo_{0.05}N$ coatings with multilayered top layer of AlTiN/CrMoN possessed higher H/E^* and H^3/E^{*2} values of up to 0.071 and 0.157, respectively. Compared to the AlTiN, the $Al_{0.29}Ti_{0.17}Cr_{0.46}Mo_{0.08}N$ and $Al_{0.38}Ti_{0.27}Cr_{0.30}Mo_{0.05}N$ coatings with nanolayered structure of the AlTiN/CrMoN top layer had high H/E^* and H^3/E^{*2} that could be beneficial to enhance the tribological and cutting performance.

It was confirmed in the cutting tests that multicomponent coatings are useful at the high-speed machining of the SUS316L stainless steels. The uncoated tool suffered serious flank wear and noticeable abrasion. The $Al_{0.63}Ti_{0.37}N$, $Al_{0.29}Ti_{0.17}Cr_{0.46}Mo_{0.08}N$ and $Al_{0.38}Ti_{0.27}Cr_{0.30}Mo_{0.05}N$ coated end mills possessed better wear resistance as a result of lower progression of tool wear. The main wear modes for the coated tools are abrasion and adhesion at the cutting edge. The hard coating of $Al_{0.38}Ti_{0.27}Cr_{0.30}Mo_{0.05}N$, which was synthesized in a multilayered structure, possessed the longest tool life. Due to its high H/E^* and H^3/E^{*2} , which exhibits high cracking resistance to improve wear performance, the $Al_{0.38}Ti_{0.27}Cr_{0.30}Mo_{0.05}N$ coating with AlTiN to CrMoN layer thickness ratio of 1.86 is suggested to be suitable for in machining of SUS316L stainless steels. The architecture and composition of the multilayered hard coating are the key parameters for the cutting applications of coated tools. Further works, including carbon addition and controlling the periodic thickness of the multilayered coatings, will be conducted.

Author Contributions: Conceptualization: Y.-Y.C.; Validation: Y.-Y.C.; Methodology: Y.-Y.C. and C.-C.C.; Formal Analysis: Y.-Y.C.; Data Curation: Y.-Y.C. and C.-C.C.; Resources: Y.-Y.C.; Writing—Original Draft Preparation: Y.-Y.C.; Writing—Review and Editing: Y.-Y.C.; Visualization: Y.-Y.C.; Supervision: Y.-Y.C.; Project Administration: Y.-Y.C.; Funding Acquisition: Y.-Y.C. All authors have read and agreed to the published version of the manuscript.

Funding: The study was financially supported by the Ministry of Science and Technology (MOST 108-2221-E-150-020-MY3) of Taiwan. We also thank the support by the “High Entropy Materials Center” from the Featured Areas Research Center Program within the framework of the Higher Education Sprout Project by the Ministry of Education (MOE) and from the Project MOST 109-2634-F-007-024 by Ministry of Science and Technology (MOST) in Taiwan.

Acknowledgments: The instrumental assistance from the Common Lab. for Micro/Nano Sci. and Tech. of National Formosa University is sincerely appreciated.

Conflicts of Interest: The authors declare no conflict of interest. None of the authors have any financial relationship with any private company or organization.

References

1. PalDey, S.; Deevi, S.C. Single layer and multilayer wear resistant coatings of (Ti,Al) N: A review. *Mater. Sci. Eng. A* **2003**, *342*, 58–79. [[CrossRef](#)]
2. Elmkhah, H.; Zhang, T.F.; Abdollah-zadeh, A.; Kim, K.H.; Mahboubi, F. Surface characteristics for the TiAlN coatings deposited by high power impulse magnetron sputtering technique at the different bias voltages. *J. Alloys Compd.* **2016**, *688*, 820–827. [[CrossRef](#)]
3. Cao, X.; He, W.; He, G.; Liao, B.; Zhang, H.; Chen, J.; Lv, C. Sand erosion resistance improvement and damage mechanism of TiAlN coating via the bias-graded voltage in FCVA deposition. *Surf. Coat. Technol.* **2019**, *378*, 125009. [[CrossRef](#)]
4. Hao, G.; Liu, Z. Experimental study on the formation of TCR and thermal behavior of hard machining using TiAlN coated tools. *Int. J. Heat Mass Transf.* **2019**, *140*, 1–11. [[CrossRef](#)]
5. Souza, P.S.; Santos, A.J.; Cotrim, M.A.P.; Abrão, A.M.; Câmara, M.A. Analysis of the surface energy interactions in the tribological behavior of AlCrN and TiAlN coatings. *Tribol. Int.* **2020**, *146*, 106206. [[CrossRef](#)]
6. Mo, J.L.; Zhu, M.H.; Leyland, A.; Matthews, A. Impact wear and abrasion resistance of CrN, AlCrN and AlTiN PVD coatings. *Surf. Coat. Technol.* **2013**, *215*, 170–177. [[CrossRef](#)]
7. Mo, J.L.; Zhu, M.H.; Lei, B.; Leng, Y.X.; Huang, N. Comparison of tribological behaviours of AlCrN and TiAlN coatings—Deposited by physical vapor deposition. *Wear* **2007**, *263*, 1423–1429. [[CrossRef](#)]

8. Lee, S.-H.; Son, B.-S.; Park, G.-T.; Ryu, J.-S.; Lee, H. Investigation of short-term, high-temperature oxidation of AlCrN coating on WC substrate. *Appl. Surf. Sci.* **2020**, *505*, 144587. [[CrossRef](#)]
9. Lin, J.; Moore, J.J.; Wang, J.; Sproul, W.D. High temperature oxidation behavior of CrN/AlN superlattice films. *Thin Solid Films* **2011**, *519*, 2402–2408. [[CrossRef](#)]
10. Lin, J.; Mishra, B.; Moore, J.J.; Sproul, W.D. A study of the oxidation behavior of CrN and CrAlN thin films in air using DSC and TGA analyses. *Surf. Coat. Technol.* **2008**, *202*, 3272–3283. [[CrossRef](#)]
11. Tang, J.-F.; Lin, C.-Y.; Yang, F.-C.; Tsai, Y.-J.; Chang, C.-L. Effects of nitrogen-argon flow ratio on the microstructural and mechanical properties of AlCrN coatings prepared using high power impulse magnetron sputtering. *Surf. Coat. Technol.* **2020**, *386*, 125484. [[CrossRef](#)]
12. Singh, A.; Ghosh, S.; Aravindan, S. Investigation of oxidation behaviour of AlCrN and AlTiN coatings deposited by arc enhanced HIPIMS technique. *Appl. Surf. Sci.* **2020**, *508*, 144812. [[CrossRef](#)]
13. Hones, P.; Consiglio, R.; Randall, N.; Lévy, F. Mechanical properties of hard chromium tungsten nitride coatings. *Surf. Coat. Technol.* **2000**, *125*, 179–184. [[CrossRef](#)]
14. Yang, Q.; Zhao, L.R.; Patnaik, P. Erosion performance, corrosion characteristics and hydrophobicity of nanolayered and multilayered metal nitride coatings. *Surf. Coat. Technol.* **2019**, *375*, 763–772. [[CrossRef](#)]
15. Postolnyi, B.O.; Beresnev, V.M.; Abadias, G.; Bondar, O.V.; Rebouta, L.; Araujo, J.P.; Pogrebnyak, A.D. Multilayer design of CrN/MoN protective coatings for enhanced hardness and toughness. *J. Alloys Compd.* **2017**, *725*, 1188–1198. [[CrossRef](#)]
16. Yeh-Liu, L.-K.; Hsu, S.-Y.; Chen, P.-Y.; Lee, J.-W.; Duh, J.-G. Improvement of CrMoN/SiN_x coatings on mechanical and high temperature Tribological properties through biomimetic laminated structure design. *Surf. Coat. Technol.* **2020**, *393*, 125754. [[CrossRef](#)]
17. Lu, Y.-C.; Chen, H.-W.; Chang, C.-C.; Wu, C.-Y.; Duh, J.-G. Tribological properties of nanocomposite Cr-Mo-Si-N coatings at elevated temperature through silicon content modification. *Surf. Coat. Technol.* **2018**, *338*, 69–74. [[CrossRef](#)]
18. Bobzin, K.; Brögelmann, T.; Kalscheuer, C. Arc PVD (Cr, Al, Mo)N and (Cr, Al, Cu)N coatings for mobility applications. *Surf. Coat. Technol.* **2020**, *384*, 125046. [[CrossRef](#)]
19. Gilewicz, A.; Warcholinski, B. Deposition and characterisation of Mo₂N/CrN multilayer coatings prepared by cathodic arc evaporation. *Surf. Coat. Technol.* **2015**, *279*, 126–133. [[CrossRef](#)]
20. Yang, Q. Wear resistance and solid lubricity of molybdenum-containing nitride coatings deposited by cathodic arc evaporation. *Surf. Coat. Technol.* **2017**, *332*, 283–295. [[CrossRef](#)]
21. Klimashin, F.; Riedl, H.; Primetzhofer, D.; Paulitsch, J.; Mayrhofer, P.H. Composition driven phase evolution and mechanical properties of Mo-Cr-N hard coatings. *J. Appl. Phys.* **2015**, *118*, 025305. [[CrossRef](#)]
22. Choi, E.Y.; Kang, M.C.; Kwon, D.H.; Shin, D.W.; Kim, K.H. Comparative studies on microstructure and mechanical properties of CrN, Cr-C-N and Cr-Mo-N coatings. *J. Mater. Process. Technol.* **2007**, *187–188*, 566–570. [[CrossRef](#)]
23. Zha, X.; Chen, F.; Jiang, F.; Xu, X. Correlation of the fatigue impact resistance of bilayer and nanolayered PVD coatings with their cutting performance in machining Ti6Al4V. *Ceram. Int.* **2019**, *45*, 14704–14717. [[CrossRef](#)]
24. Vereschaka, A.A.; Grigoriev, S.N.; Sitnikov, N.N.; Batako, A.D. Delamination and longitudinal cracking in multi-layered composite nano-structured coatings and their influence on cutting tool life. *Wear* **2017**, *390–391*, 209–219. [[CrossRef](#)]
25. Shuai, J.; Zuo, X.; Wang, Z.; Guo, P.; Xu, B.; Zhou, J.; Wang, A.; Ke, P. Comparative study on crack resistance of TiAlN monolithic and Ti/TiAlN multilayer coatings. *Ceram. Int.* **2020**, *46*, 6672–6681. [[CrossRef](#)]
26. Chang, Y.-Y.; Yang, Y.-J.; Weng, S.-Y. Effect of interlayer design on the mechanical properties of AlTiCrN and multilayered AlTiCrN/TiSiN hard coatings. *Surf. Coat. Technol.* **2020**, *389*, 125637. [[CrossRef](#)]
27. Chang, Y.-Y.; Wu, C.-J. Mechanical properties and impact resistance of multilayered TiAlN/ZrN coatings. *Surf. Coat. Technol.* **2013**, *231*, 62–66. [[CrossRef](#)]
28. Qiu, L.; Du, Y.; Wu, L.; Wang, S.; Zhu, J.; Cheng, W.; Tan, Z.; Yin, L.; Liu, Z.; Layyous, A. Microstructure, mechanical properties and cutting performances of TiSiCN super-hard nanocomposite coatings deposited using CVD method under the guidance of thermodynamic calculations. *Surf. Coat. Technol.* **2019**, *378*, 124956. [[CrossRef](#)]
29. Vereschaka, A.A.; Grigoriev, S.N.; Sitnikov, N.N.; Oganyan, G.V.; Batako, A. Working efficiency of cutting tools with multilayer nano-structured Ti-TiCN-(Ti,Al)CN and Ti-TiCN-(Ti,Al,Cr)CN coatings: Analysis

- of cutting properties, wear mechanism and diffusion processes. *Surf. Coat. Technol.* **2017**, *332*, 198–213. [[CrossRef](#)]
30. Sanchette, F.; Ducros, C.; Schmitt, T.; Steyer, P.; Billard, A. Nanostructured hard coatings deposited by cathodic arc deposition: From concepts to applications. *Surf. Coat. Technol.* **2011**, *205*, 5444–5453. [[CrossRef](#)]
 31. Deng, Y.; Chen, W.; Li, B.; Wang, C.; Kuang, T.; Li, Y. Physical vapor deposition technology for coated cutting tools: A review. *Ceram. Int.* **2020**, *46*, 18373–18390. [[CrossRef](#)]
 32. Sanders, D.M.; Anders, A. Review of cathodic arc deposition technology at the start of the new millennium. *Surf. Coat. Technol.* **2000**, *133–134*, 78–90. [[CrossRef](#)]
 33. Kutschej, K.; Mayrhofer, P.H.; Kathrein, M.; Polcik, P.; Tessadri, R.; Mitterer, C. Structure, mechanical and tribological properties of sputtered Ti_{1-x}Al_xN coatings with 0.5 ≤ x ≤ 0.75. *Surf. Coat. Technol.* **2005**, *200*, 2358–2365. [[CrossRef](#)]
 34. Chang, Y.-Y.; Wang, D.-Y. Characterization of nanocrystalline AlTiN coatings synthesized by a cathodic-arc deposition process. *Surf. Coat. Technol.* **2007**, *201*, 6699–6701. [[CrossRef](#)]
 35. Chang, Y.-Y.; Chang, C.-P.; Kao, H.-Y. High temperature oxidation resistance of multilayered Al_xTi_{1-x}N/CrN coatings. *Thin Solid Films* **2011**, *519*, 6716–6720. [[CrossRef](#)]
 36. Gao, B.; Du, X.; Li, Y.; Wei, S.; Zhu, X.; Song, Z. Effect of deposition temperature on hydrophobic CrN/AlTiN nanolaminate composites deposited by Multi-Arc-Ion Plating. *J. Alloys Compd.* **2019**, *797*, 1–9. [[CrossRef](#)]
 37. Mo, J.; Wu, Z.; Yao, Y.; Zhang, Q.; Wang, Q. Influence of Y-addition and multilayer modulation on microstructure, oxidation resistance and corrosion behavior of Al_{0.67}Ti_{0.33}N coatings. *Surf. Coat. Technol.* **2018**, *342*, 129–136. [[CrossRef](#)]
 38. Yang, Q.; McKellar, R. Nanolayered CrAlTiN and multilayered CrAlTiN–AlTiN coatings for solid particle erosion protection. *Tribol. Int.* **2015**, *83*, 12–20. [[CrossRef](#)]
 39. Liu, Z.R.; Xu, Y.X.; Peng, B.; Wei, W.; Chen, L.; Wang, Q. Structure and property optimization of Ni-containing AlCrSiN coatings by nano-multilayer construction. *J. Alloys Compd.* **2019**, *808*, 151630. [[CrossRef](#)]
 40. Zhang, Q.; Wu, Z.; Xu, Y.X.; Wang, Q.; Chen, L.; Kim, K.H. Improving the mechanical and anti-wear properties of AlTiN coatings by the hybrid arc and sputtering deposition. *Surf. Coat. Technol.* **2019**, *378*, 125022. [[CrossRef](#)]
 41. Wang, L.; Wang, M.; Chen, H. Corrosion mechanism investigation of TiAlN/CrN superlattice coating by multi-arc ion plating in 3.5 wt% NaCl solution. *Surf. Coat. Technol.* **2020**, *391*, 125660. [[CrossRef](#)]
 42. Sadeghi-Khosravieh, S.; Robbie, K. Morphology and crystal texture in tilted columnar micro-structured titanium thin film coatings. *Thin Solid Films* **2017**, *627*, 69–76. [[CrossRef](#)]
 43. von Fieandt, K.; Riekehr, L.; Osinger, B.; Fritze, S.; Lewin, E. Influence of N content on structure and mechanical properties of multi-component Al-Cr-Nb-Y-Zr based thin films by reactive magnetron sputtering. *Surf. Coat. Technol.* **2020**, *389*, 125614. [[CrossRef](#)]
 44. Chen, L.; Xu, Y.X.; Du, Y.; Liu, Y. Effect of bilayer period on structure, mechanical and thermal properties of TiAlN/AlTiN multilayer coatings. *Thin Solid Films* **2015**, *592*, 207–214. [[CrossRef](#)]
 45. Tillmann, W.; Fehr, A.; Stangier, D.; Dildrop, M. Influences of substrate pretreatments and Ti/Cr interlayers on the adhesion and hardness of CrAlSiN and TiAlSiN films deposited on Al₂O₃ and ZrO₂-8Y₂O₃ thermal barrier coatings. *Results Phys.* **2019**, *12*, 2206–2212. [[CrossRef](#)]
 46. Du, H.; Zhao, H.; Xiong, J.; Xian, G. Effect of interlayers on the structure and properties of TiAlN based coatings on WC-Co cemented carbide substrate. *Int. J. Refract. Met. Hard Mater.* **2013**, *37*, 60–66. [[CrossRef](#)]
 47. Xu, Y.X.; Chen, L.; Pei, F.; Du, Y. Structure and thermal properties of TiAlN/CrN multilayered coatings with various modulation ratios. *Surf. Coat. Technol.* **2016**, *304*, 512–518. [[CrossRef](#)]
 48. Chang, Y.-Y.; Chang, C.-P. Microstructural and mechanical properties of graded and multilayered Al_xTi_{1-x}N/CrN coatings synthesized by a cathodic-arc deposition process. *Surf. Coat. Technol.* **2009**, *204*, 1030–1034. [[CrossRef](#)]
 49. Yashar, P.C.; Sproul, W.D. Nanometer scale multilayered hard coatings. *Vacuum* **1999**, *55*, 179–190. [[CrossRef](#)]
 50. Ziebert, C.; Stüber, M.; Leiste, H.; Ulrich, S.; Holleck, H. Nanoscale PVD Multilayer Coatings. In *Encyclopedia of Materials: Science and Technology*; Buschow, K.H.J., Cahn, R.W., Flemings, M.C., Ilschner, B., Kramer, E.J., Mahajan, S., Veyssi re, P., Eds.; Elsevier: Oxford, UK, 2011; pp. 1–8.
 51. Lin, Y.-W.; Chih, P.-C.; Huang, J.-H. Effect of Ti interlayer thickness on mechanical properties and wear resistance of TiZrN coatings on AISI D2 steel. *Surf. Coat. Technol.* **2020**, *394*, 125690. [[CrossRef](#)]

52. Sprute, T.; Tillmann, W.; Grisales, D.; Selvadurai, U.; Fischer, G. Influence of substrate pre-treatments on residual stresses and tribo-mechanical properties of TiAlN-based PVD coatings. *Surf. Coat. Technol.* **2014**, *260*, 369–379. [[CrossRef](#)]
53. Wang, Q.; Zhou, F.; Zhou, Z.; Li, L.K.-Y.; Yan, J. An investigation on the crack resistance of CrN, CrBN and CrTiBN coatings via nanoindentation. *Vacuum* **2017**, *145*, 186–193. [[CrossRef](#)]
54. Musil, J.; Kunc, F.; Zeman, H.; Poláková, H. Relationships between hardness, Young's modulus and elastic recovery in hard nanocomposite coatings. *Surf. Coat. Technol.* **2002**, *154*, 304–313. [[CrossRef](#)]
55. Leyland, A.; Matthews, A. On the significance of the H/E ratio in wear control: A nanocomposite coating approach to optimised tribological behaviour. *Wear* **2000**, *246*, 1–11. [[CrossRef](#)]
56. Musil, J. Hard nanocomposite coatings: Thermal stability, oxidation resistance and toughness. *Surf. Coat. Technol.* **2012**, *207*, 50–65. [[CrossRef](#)]
57. Ou, Y.X.; Ouyang, X.P.; Liao, B.; Zhang, X.; Zhang, S. Hard yet tough CrN/Si₃N₄ multilayer coatings deposited by the combined deep oscillation magnetron sputtering and pulsed dc magnetron sputtering. *Appl. Surf. Sci.* **2020**, *502*, 144168. [[CrossRef](#)]
58. Zhang, K.; Guo, X.; Sun, L.; Meng, X.; Xing, Y. Fabrication of coated tool with femtosecond laser pretreatment and its cutting performance in dry machining SLM-produced stainless steel. *J. Manuf. Process.* **2019**, *42*, 28–40. [[CrossRef](#)]
59. Endrino, J.L.; Fox-Rabinovich, G.S.; Gey, C. Hard AlTiN, AlCrN PVD coatings for machining of austenitic stainless steel. *Surf. Coat. Technol.* **2006**, *200*, 6840–6845. [[CrossRef](#)]
60. Lai, Z.; Wang, C.; Zheng, L.; Huang, W.; Yang, J.; Guo, G.; Xiong, W. Adaptability of AlTiN-based coated tools with green cutting technologies in sustainable machining of 316L stainless steel. *Tribol. Int.* **2020**, *148*, 106300. [[CrossRef](#)]
61. Zhang, K.; Deng, J.; Sun, J.; Jiang, C.; Liu, Y.; Chen, S. Effect of micro/nano-scale textures on anti-adhesive wear properties of WC/Co-based TiAlN coated tools in AISI 316 austenitic stainless steel cutting. *Appl. Surf. Sci.* **2015**, *355*, 602–614. [[CrossRef](#)]
62. Wang, T.; Zhang, J.; Li, Y.; Gao, F.; Zhang, G. Self-lubricating TiN/MoN and TiAlN/MoN nano-multilayer coatings for drilling of austenitic stainless steel. *Ceram. Int.* **2019**, *45*, 24248–24253. [[CrossRef](#)]
63. Beake, B.D.; Ning, L.; Gey, C.; Veldhuis, S.C.; Komarov, A.; Weaver, A.; Khanna, M.; Fox-Rabinovich, G.S. Wear performance of different PVD coatings during hard wet end milling of H13 tool steel. *Surf. Coat. Technol.* **2015**, *279*, 118–125. [[CrossRef](#)]
64. Varghese, V.; Chakradhar, D.; Ramesh, M.R. Micro-mechanical characterization and wear performance of TiAlN/NbN PVD coated carbide inserts during End milling of AISI 304 Austenitic Stainless Steel. *Mater. Today Proc.* **2018**, *5*, 12855–12862. [[CrossRef](#)]
65. Bag, R.; Panda, A.; Sahoo, A.K.; Kumar, R. Cutting tools characteristics and coating depositions for hard part turning of AISI 4340 martensitic steel: A review study. *Mater. Today Proc.* **2020**, *26*, 2073–2078. [[CrossRef](#)]
66. Li, G.; Li, L.; Han, M.; Luo, S.; Jin, J.; Wang, L.; Gu, J.; Miao, H.J.M. The performance of TiAlSiN coated cemented carbide tools enhanced by inserting Ti interlayers. *Metals* **2019**, *9*, 918. [[CrossRef](#)]

